

Meteorology and Ozone, Temperature, Relative Humidity

J. Coates¹ and T. Butler¹

¹Institute for Advanced Sustainability Studies, Potsdam, Germany

December 23, 2015

Abstract

1 Introduction

Surface-level ozone (O_3) is a secondary air pollutant formed from the photochemical degradation of volatile organic compounds (VOCs) in the presence of nitrogen oxides (NO_x). Due to the photochemical nature of ozone production, meteorological factors such as temperature strongly influence ozone production (Jacob and Winner, 2009). Temperature influences ozone production through temperature-dependent emissions of VOC from biogenic sources (anthropogenic emissions are typically not temperature dependent) and the reaction rates of many of the chemical reactions involved in producing ozone are also temperature dependent. The recent review of Pusede et al. (2015) provides a detailed description of the temperature-dependent processes impacting ozone production. A recent study by indicates that temperature is a major meteorological driver for ozone in central europe.

Many studies over the US (Sillman and Samson, 1995; Dawson et al., 2007; Pusede et al., 2014) have observed the relationship between ozone and temperature, noting that increased temperatures tend to lead to higher ozone levels, often exceeding local air quality guidelines. Some of these studies (Sillman and Samson, 1995; Dawson et al., 2007) include modelling experiments using regional chemical transport models which have indeed verified the observed increases in ozone with temperature. The increase in the thermal decomposition rate of PAN (peroxy acetyl nitrate) with temperature is commonly cited for the increase of ozone with temperature.

Noelia's
paper

Environmental chamber studies have looked at the relationship of ozone with temperature using a particular mixture of VOCs. The chamber experiments of Carter et al. (1979) and Hatakeyama et al. (1991), also showed increases in ozone with temperature and have also linked this relationship to increased PAN decomposition at higher temperatures ($T > 303$ K). Hatakeyama et al. (1991) looked primarily at the influence of HO_2NO_2 decomposition on ozone production and induced that at lower temperatures ($T < 303$ K) HO_2NO_2 decomposition has a large influence on ozone production but the influence of PAN decomposition on ozone production increases with temperature.

Pusede et al. (2014) used observations over the San Joaquin Valley, California to infer a non-linear relationship of ozone production with temperature and NO_x , similar to the well-known non-linear relationship of ozone production on NO_x and VOC levels (Sillman, 1999). In fact, Pusede et al. (2014) show that temperature can be used as a surrogate for VOC levels when looking at the relationship of ozone across NO_x gradients. Moreover, the described relationship of ozone on both NO_x and temperature needs to be considered when looking at effective strategies to reduce levels of surface ozone.

Despite a wealth of studies looking at the effects of temperature on ozone chemistry, there have not been (to our knowledge) modelling studies focusing on these effects across different NO_x gradients and whether the observed relationships are well-represented by different chemical mechanisms used in air quality models. The review of Pusede et al. (2015) also highlights a lack of modelling studies looking at this non-linear relationship of ozone on temperature across NO_x gradients. In this study, we use an idealised box model to determine how ozone levels vary with temperature and across NO_x gradients. We separate the effects of temperature-dependent chemistry and VOC emissions on ozone production by performing simulations including a temperature-independent source of isoprene followed by simulations using a temperature-dependent source of isoprene.

The study of Rasmussen et al. (2013) looking at the change of ozone with temperature in California (termed the “Ozone-Climate Penalty”) indicates that changing the chemical mechanism used by a model may also change the Ozone-Climate Penalty and should be investigated. Finally, by repeating these simulations with different chemical mechanisms, we determine whether the temperature dependence of ozone production is reproduced across different NO_x gradients in these chemical mechanisms.

2 Methodology

2.1 Model Setup

- MECCA box model as described in Coates and Butler (2015) to broadly simulate the Benelux (Belgium, Netherlands and Luxembourg) region. As photolysis rates are parameterised by the solar zenith angle, the solar zenith angle of 51°N was used, representative of the central Benelux region.
- MECCA box model has been updated to include vertical mixing with the free troposphere and accordingly includes a diurnal cycle for the PBL height. These amendments are discussed further in Sect. 2.4.
- Simulations start at 06:00 using spring equinoctical conditions and the simulations ended after two days.
- All simulations performed using the Master Chemical Mechanism, MCM v3.2, (Rickard et al., 2015), Common Representative Intermediates, CRI v2 (Jenkin et al., 2008), Model for Ozone and related chemical tracers, MOZART-4 (Emmons et al., 2010), Regional Acid Deposition Model, RADM2 (Stockwell et al., 1990) and the Carbon Bond Mechanism, CB05 (Yarwood et al., 2005). Coates and Butler (2015) describes the implementation of these chemical mechanisms for use with KPP within MECCA. These chemical mechanisms were chosen as they are commonly used by modelling groups and represent the highly-detailed chemistry (MCM v3.2), chemistry suitable for regional 3D models (CRI v2, RADM2 and CB05) and global 3D models (MOZART-4).
- NO_x emissions and temperature were varied systematically to analyse the effects on ozone mixing ratios over different NO_x gradients at each temperature.
- VOC emissions constant until noon of first day, to simulate a plume of emitted VOC.
- Two sets of runs were performed – to include both a temperature-dependent and temperature-independent source of biogenic VOC emissions. MEGANv2.1 (Guenther et al., 2012) was used to specify the temperature-dependent BVOC emissions of isoprene. Isoprene is the most important VOC at a global scale due its high emission rates and emissions from vegetation have been reported to depend on temperature (Guenther et al.,

2006). In reality, increased temperature can also increase AVOC emissions by increasing evaporation of NMVOCs, this is not included in our study.

- Methane is fixed at 1.7 ppmv throughout the model run, carbon monoxide (CO) and ozone were initialised at 200 ppbv and 40 ppbv and then allowed to evolve freely throughout the the simulation.
- The temperature was systematically varied between 288 and 313 K (15 – 40 °C). The only source of NOx emissions in the box model was a constant source of NO emissions. The NO emissions were systematically varied from 5.0×10^9 to 1.5×10^{12} molecules (NO) $\text{cm}^{-2} \text{s}^{-1}$ at each temperature used in this study.

2.2 VOC Emissions

- Anthropogenic emissions from Benelux for the year 2011 were obtained from the TNO-MACC_III emission inventory. TNO-MACC_III is the current version of the TNO-MACC_II inventory and was created using the same methodology as Kuenen et al. (2014) and based upon improvements to the existing emission inventory during the AQMEII-2 exercises described in Pouliot et al. (2015).
- Temperature-independent emissions of the biogenic VOC isoprene and monoterpenes, were calculated as a fraction of the total anthropogenic VOC emissions from each country in the Benelux region, this data was obtained from the supplementary data available from the EMEP (European Monitoring and Evaluation Programme) model (Simpson et al., 2012).
- AVOC and BVOC emissions are included as total emissions from SNAP (Selected Nomenclature for Air Pollution) source categories and these emissions were assigned to chemical groupings based on the country specific profiles for Belgium, the Netherlands and Luxembourg provided by TNO.
- The MCM v3.2 initial species were determined using the country specific profiles for each SNAP source category and where appropriate information of individual chemical species that can be represented by MCM v3.2 were determined using the detailed speciations of Passant (2002). This approach was also used in von Schneidemesser et al. (2015) and further details are found within this article.

Table 1: Total anthropogenic NMVOC emissions in 2011 in tonnes from each SNAP category assigned from TNO-MACC_III emission inventory and biogenic VOC emission in tonnes from Benelux region assigned from EMEP. The allocation of these emissions to MCM v3.2, CRI v2, CB05, MOZART-4 and RADM2 species is found in the supplement.

	SNAP1	SNAP2	SNAP34	SNAP5	SNAP6	SNAP71
Belgium	4494	9034	22152	5448	42809	6592
Netherlands	9140	12173	29177	8723	53535	16589
Luxembourg	121	44	208	1371	4482	1740
Total	13755	21251	62648	15542	100826	24921
	SNAP72	SNAP73	SNAP74	SNAP8	SNAP9	BVOC
Belgium	2446	144	210	6448	821	7042
Netherlands	3230	1283	1793	10067	521	1462
Luxembourg	1051	6	324	643	0	2198
Total	6727	1433	2327	17158	1342	10702

- As in von Schneidemesser et al. (2015), first the primary VOC that are represented by the MCM v3.2 and respective emissions were determined. Using this MCM v3.2 data, the NMVOC emission data were mapped to mechanism species in the other four chemical mechanisms used in the study. The NMVOC emissions in the non-MCM v3.2 chemical mechanisms were weighted by the carbon numbers of the MCM v3.2 species and the emitted mechanism species. The supplementary data outlines the primary NMVOC and calculated emissions with each chemical mechanism.

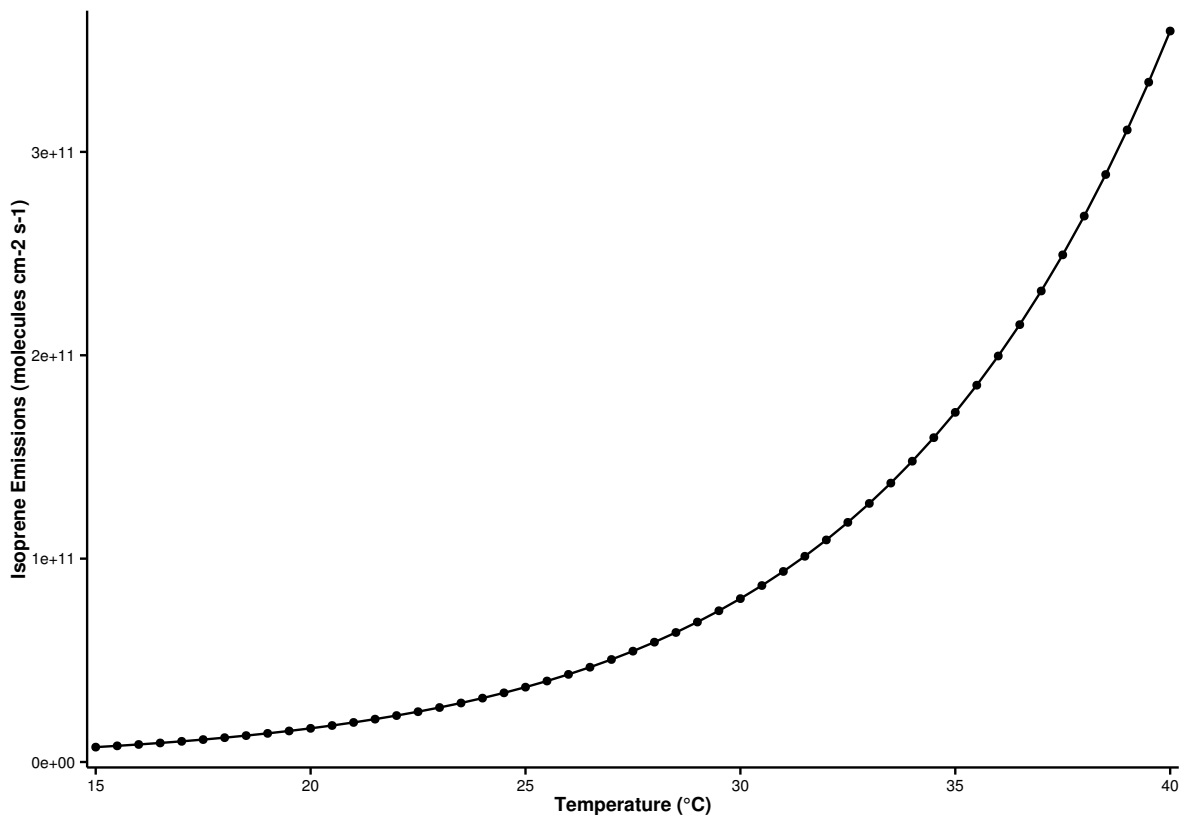
2.3 Temperature Dependent Isoprene Emissions

- Temperature dependent isoprene emissions were estimated using the MEGAN2.1 algorithm (Guenther et al., 2012).
- The aim of the study is to look at the effects of temperature, hence in the MEGAN2.1 algorithm all parameters (except temperature) were kept constant.
- The boxmodel setup uses a constant temperature throughout the model run and so the parameters T_{24} and T_{240} , the average temperatures in the past 24 and 250 hours, were assumed to be constant and equal to the temperature value of the boxmodel.
- Constant PAR (photosynthetically active radiation) and LAI (leaf area index) were used at each temperature step.
- The LAI, plant functional type (PFT) and associated isoprene emission factor were taken from Guenther et al. (2012) and selected to give the same isoprene mixing ratios at a temperature of 293 K as in the temperature independent modelling case. For all other model runs over the different temperature, the MEGAN2.1 algorithm was used to estimate the isoprene emissions.
- Thus using this idealised case, we can determine the effects of increasing isoprene emissions with temperature across NO_x gradients.
- This was repeated for each chemical mechanism.
- As in the temperature independent model runs, the emissions of NMVOC and the temperature dependent source of isoprene, were held constant until noon of the first day.
- Using these assumptions, the isoprene emissions at each temperature step of the study are illustrated in Fig. 1 and show the expected exponential increase in emissions with temperature (Guenther et al., 2006).

2.4 Vertical Mixing with Diurnal Boundary Layer Height

- The MECCA box model used in Coates and Butler (2015) included a constant boundary layer height of 1 km and no interactions (vertical mixing) with the free troposphere.

Figure 1: The estimated isoprene emissions (molecules isoprene $\text{cm}^{-2} \text{s}^{-1}$) at each temperature step used in the study. Isoprene emissions were estimated using the MEGAN2.1 algorithm (Guenther et al., 2012).



- The planetary boundary layer (PBL) height varies diurnally and affects chemistry by diluting emissions after sunrise when the PBL rises. The expansion of the PBL into the free troposphere introduces vertical mixing with those chemical species present in the free troposphere. When the PBL collapses in the evening, pollutants are trapped in the PBL.
- The mixing layer height was measured as part of the BAERLIN campaign over the city of Berlin, Germany. The profile of mean mixing layer height during the campaign period (June – August 2014) was used in the model to represent the diurnal cycle of the mixing layer height.
- The concentrations of the chemical species within the PBL are diluted due to the larger mixing volume when the PBL height increases at the beginning of the day, also the increasing PBL height mixes the chemical species from the free troposphere with the chemical species within the PBL i.e. vertical mixing. The PBL height collapses during night leaving the stable nocturnal boundary layer, trapping the chemical species into a smaller volume thus increasing the concentrations of the chemical species.

Reference
Boris'
paper

Table 2: Increase in ozone mixing ratio (ppbv) due to chemistry and emissions at 40 °C from reference temperature (20 °C) in the NO_x-regimes of Fig. 2.

Chemical Mechanism	Source of Difference	Increase in Ozone at 40 °C from 20 °C (ppbv)		
		Low-NO _x	Maximal-O ₃	High-NO _x
MCMv3.2	Chemistry	6.8	12.5	15.2
	Emissions	4.6	7.7	10.6
CRIV2	Chemistry	6.0	11.1	13.7
	Emissions	4.8	7.9	10.8
MOZART-4	Chemistry	6.0	10.2	12.3
	Emissions	4.1	6.7	10.0
CB05	Chemistry	9.3	16.0	19.9
	Emissions	4.6	7.4	9.8
RADM2	Chemistry	8.6	14.1	17.3
	Emissions	3.8	5.7	7.8

- This vertical mixing scheme was implemented into the boxmodel using the same approach of Lourens (2012).
- The mixing ratios of O₃, CO and CH₄ in the free troposphere were respectively set to 50 ppbv, 116 ppbv and 1.8 ppmv. These conditions were taken from the MATCH-MPIC chemical weather forecast model on the 21st March (the start date of the simulations). The model results (<http://cwfiass-potsdam.de/>) at the 700 hPa height were chosen and the daily average was used as input into the boxmodel.

check
reference

3 Results

3.1 Ozone mixing ratios as function of NO_x and Temperature

Figure 2 depicts the maximum mixing ratio of ozone as a function of the total NO_x emissions on the first day and temperature when using temperature-independent and temperature-dependent source of isoprene emissions for each chemical mechanism. A non-linear relationship of ozone mixing ratios with NO_x and temperature is reproduced by each chemical mechanism.

The highest mixing ratios of ozone in Fig. 2 are produced at higher temperatures and high-NO_x conditions, also ozone mixing ratios increase when using a temperature-dependent source of isoprene emissions. Conversely, the least amount of ozone is produced with low-NO_x conditions over the whole temperature range (15 – 40 °C) when using both a temperature-independent and temperature-dependent source of isoprene emissions.

The non-linear relationship of ozone with NO_x and temperature can be split into three NO_x-regimes (low-NO_x, maximal-O₃ and high-NO_x) based on the ratio of HNO₃ to H₂O₂ used in

Figure 2: Contours of maximum ozone mixing ratio as a function of the total NO_x emissions on the first day and temperature for each chemical mechanism and using both a temperature-dependent and -independent source of isoprene emissions.

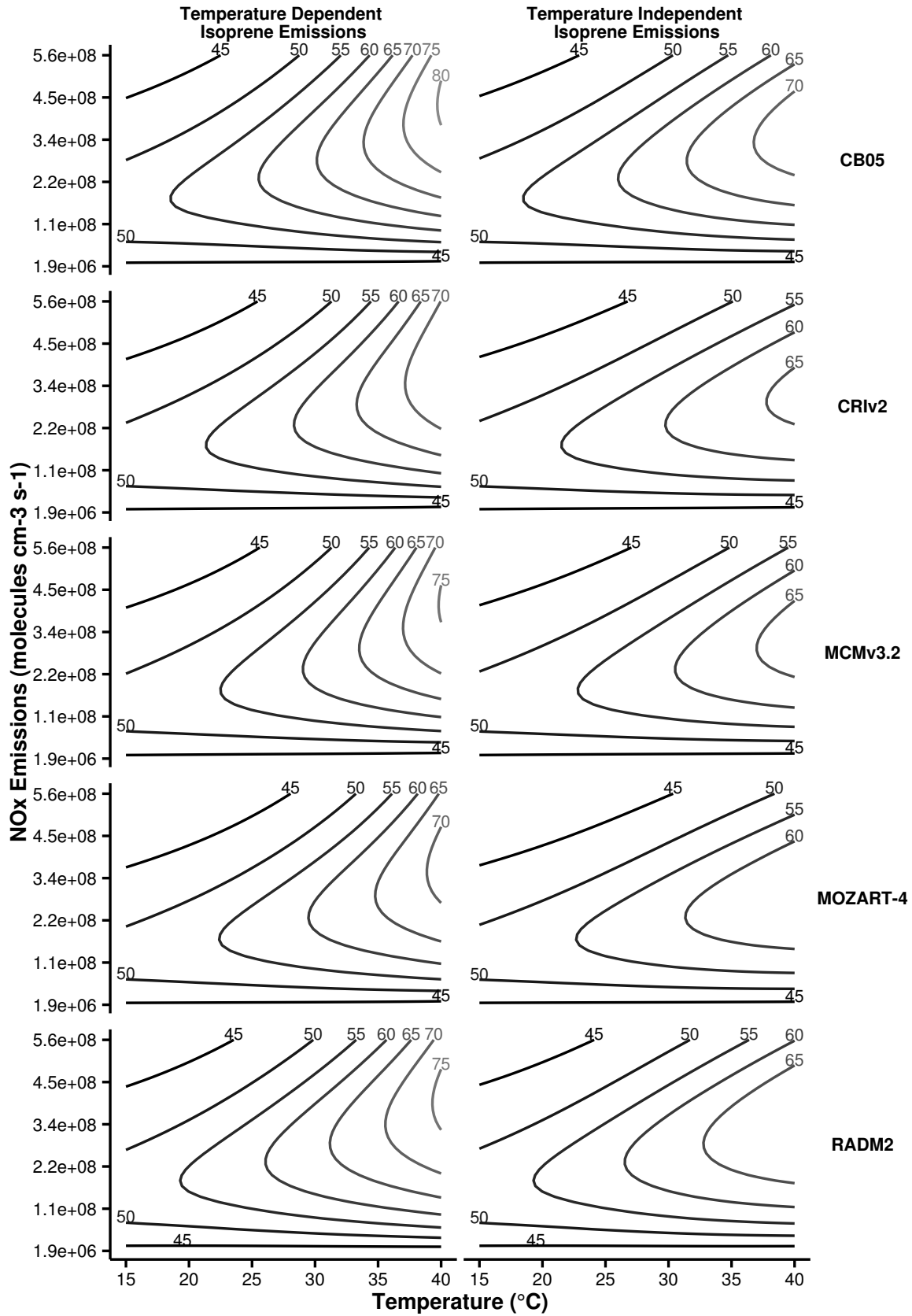
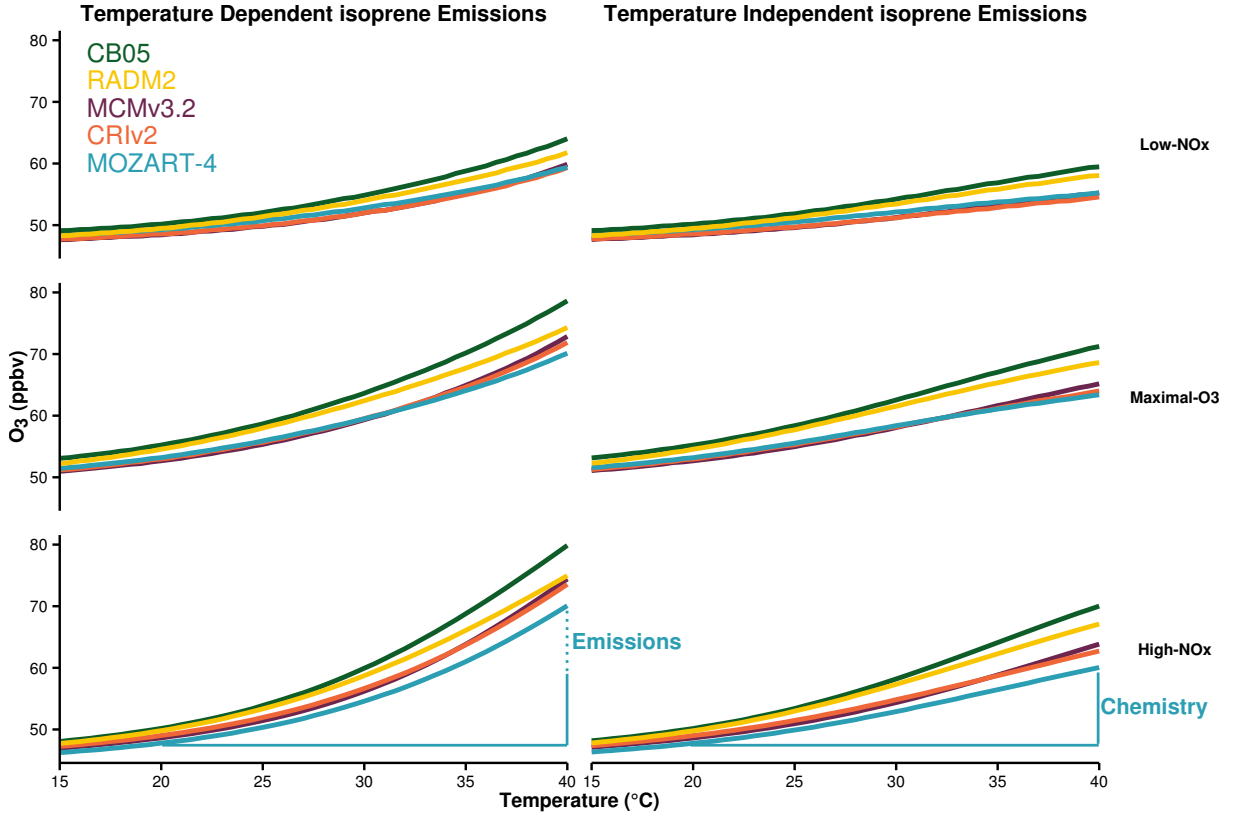


Figure 3: Ozone mixing ratios at each temperature are allocated to different NO_x -regimes of Fig. 2. The differences in ozone mixing ratios due to chemistry and emissions of Table 2 are represented graphically for MOZART-4, the approach was used to calculate the differences with each chemical mechanism.



Sillman (1995) to determine NO_x -regimes for the non-linear relationship of ozone with NO_x and VOC. The low- NO_x regime corresponds to the lower-left most area in Fig. 2 where there is little increase in ozone with temperature, also called NO_x -sensitive conditions. The high- NO_x regime is when ozone levels increase rapidly with temperature in Fig. 2, sometimes called NO_x -saturated conditions. Finally, the ridges of the contours in Fig. 2 correspond to maximal-ozone production and we call this the maximal- O_3 regime. The ozone mixing ratios obtained in each simulation were assigned to a NO_x regime based on the $\text{H}_2\text{O}_2:\text{HNO}_3$ of the simulation and Fig. 3 illustrates the mean ozone mixing ratio at each temperature in these NO_x regimes.

Calculating the difference in ozone mixing ratios at 40 $^{\circ}\text{C}$ from 20 $^{\circ}\text{C}$ when using a temperature-independent source of isoprene emissions gives the absolute increase in ozone due to faster chemistry. When using a temperature-dependent source of isoprene emissions, the difference in ozone mixing ratios at 40 $^{\circ}\text{C}$ from 20 $^{\circ}\text{C}$ less the increase due to faster chemistry, gives the absolute increase in ozone due to increased isoprene emissions. These differences are represented graphically in Fig. 3 and summarised in Table 2.

Both Fig. 3 and Table 2 highlight that the absolute increase in ozone at 40 $^{\circ}\text{C}$ from 20 $^{\circ}\text{C}$ is

largest with high-NO_x conditions. The increase in ozone mixing ratio at 40 °C from 20 °C due to faster chemistry with high-NO_x conditions is almost double that with low-NO_x conditions. We shall explore which chemical processes are responsible for the increases in ozone mixing ratios at 40 °C from 20 °C by analysing O_x production budgets in Sect. 3.2.

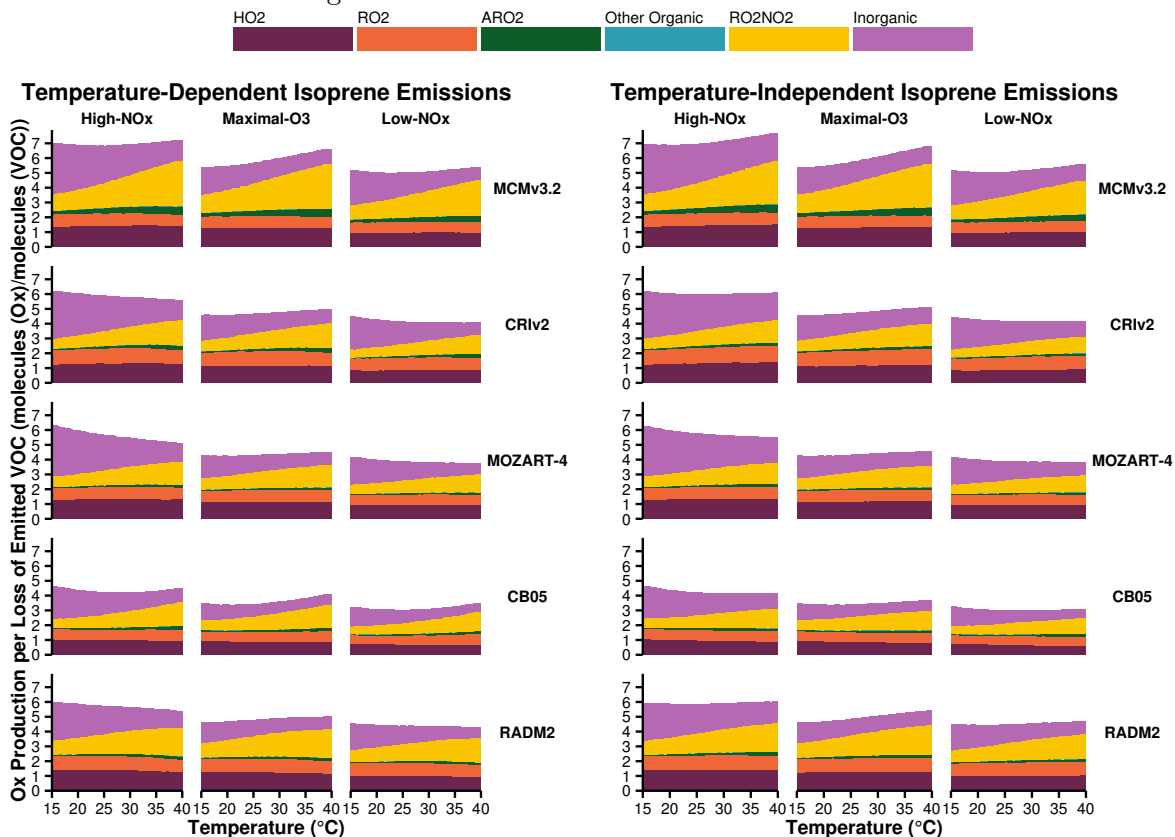
Comparing the response of ozone mixing ratios to temperature in the reduced chemical mechanisms (CRIV2, MOZART-4, CB05 and RADM2) to the near-explicit MCMv3.2 chemical mechanism shows that the largest differences from the MCMv3.2 occur in the maximal-O₃ and high-NO_x regimes. Table 2 also indicates that all reduced chemical mechanisms, except RADM2, have similar increases in ozone due to temperature-dependent isoprene emissions to MCMv3.2. RADM2 produces 3 ppbv less ozone than the MCMv3.2 due to temperature-dependent isoprene emissions consistently in each NO_x regime, indicating that this difference is due to how isoprene degradation chemistry is treated in RADM2.

The Tagged Ozone Production Potential (TOPP) of isoprene is a measure of the number of molecules of ozone produced per molecule of isoprene emitted and Coates and Butler (2015) shows that less ozone is produced from isoprene degradation using RADM2 than with MCMv3.2. The degradation of isoprene has been extensively studied and it is well-known that the species methyl vinyl ketone (MVK) and methacrolein are signatures of isoprene degradation. All chemical mechanisms used in our study do explicitly include MVK and methacrolein (or in the case of CB05, a lumped species representing both these secondary degradation products) production during isoprene degradation except RADM2. RADM2 does not include methacrolein and the ketone species included in RADM2 represents a mixture of acetone and methyl ethyl ketone (MEK), thus the secondary degradation of isoprene in RADM2 is unable to represent the ozone production from the further degradation of its signature degradation products MVK and methacrolein. More recent versions of RADM2, RACM (Stockwell et al., 1997) and RACM2 (Goliff et al., 2013), sequentially include methacrolein and MVK and with these updates the TOPP values of isoprene reported in Coates and Butler (2015) are similar to the TOPP value of isoprene in the MCMv3.2.

3.2 Ozone Production Budgets

In order to determine which chemical processes are causing the increase in ozone with temperature (Sect. 3.1), we analyse the O_x production budgets in each NO_x regime (low-NO_x, Maximal-O₃ and high-NO_x) defined in Sect. 3.1. We defined the O_x family to consist of O₃, NO₂ and O, and Fig. 4 displays the total day-time O_x production budgets normalised by the total initial

Figure 4: Day-time O_x production budgets normalised by the total oxidation rate of emitted VOC in the NO_x -regimes of Fig. 2. The budgets are allocated to the categories of inorganic reactions, peroxy nitrate (RO_2NO_2) decomposition, reactions of NO with HO_2 , alkyl peroxy radicals (RO_2) and acyl peroxy radicals (ARO_2). All other reactions contributing to O_x budgets are allocated to ‘Other Organic’.



oxidation rates of the emitted NMVOC for each chemical mechanism within each NO_x regime. The O_x production budgets in Fig. 4 are allocated to the major sources, where ‘ HO_2 ’, ‘ RO_2 ’, ‘ ARO_2 ’ represent the reactions of NO with HO_2 , alkyl peroxy radicals and acyl peroxy radicals respectively. ‘ RO_2NO_2 ’ represents the thermal decomposition of peroxy nitrates, ‘Inorganic’ represents all inorganic contributions to the O_x production budgets (primarily the de-excitation of O^1D to O) and any other remaining organic reactions producing O_x are included in the ‘Other Organic’ category.

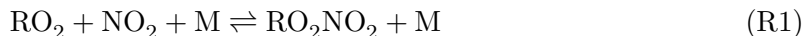
In Fig. 4 the number of molecules of O_x produced per molecule of NMVOC oxidised in High- NO_x conditions is similar when using temperature-dependent or temperature-independent isoprene emissions for each chemical mechanism; the same is also true for the Maximal- O_3 and Low- NO_x regimes. Thus the increases in isoprene emissions in the temperature-dependent simulations are balanced by the faster oxidation rates of the emitted NMVOC. The highest amount of O_x is produced in the High- NO_x regime and the lowest amount of O_x is produced in

the Low- NO_x regime, mirroring the O_3 mixing ratios in the different NO_x regimes in Fig.3. For example, when using MCMv3.2 seven molecules of O_x are produced per molecule of NMVOC oxidation in High- NO_x conditions, decreased to about six and five molecules of O_x produced per molecule of NMVOC oxidised in the Maximal- O_3 and Low- NO_x regimes. In each NO_x regime, all the reduced chemical mechanisms produce up to two molecules of O_x per molecule of emitted NMVOC oxidised less than the MCMv3.2.

Turning to the individual contributions to the normalised production of O_x in Fig. 4, peroxy nitrate (RO_2NO_2) decomposition and inorganic reactions show a strong (and opposing) dependence on temperature in all NO_x regimes, each chemical mechanism and regardless of the source of isoprene emissions. Whereas the contributions of the reaction of NO with the peroxy radicals (HO_2 , RO_2 and ARO_2 in Fig. 4) to the normalised production budgets of O_x do not increase strongly with temperature indicating that these processes are strongly related to the faster oxidation of the emitted NMVOC with temperature.

3.2.1 Peroxynitrates

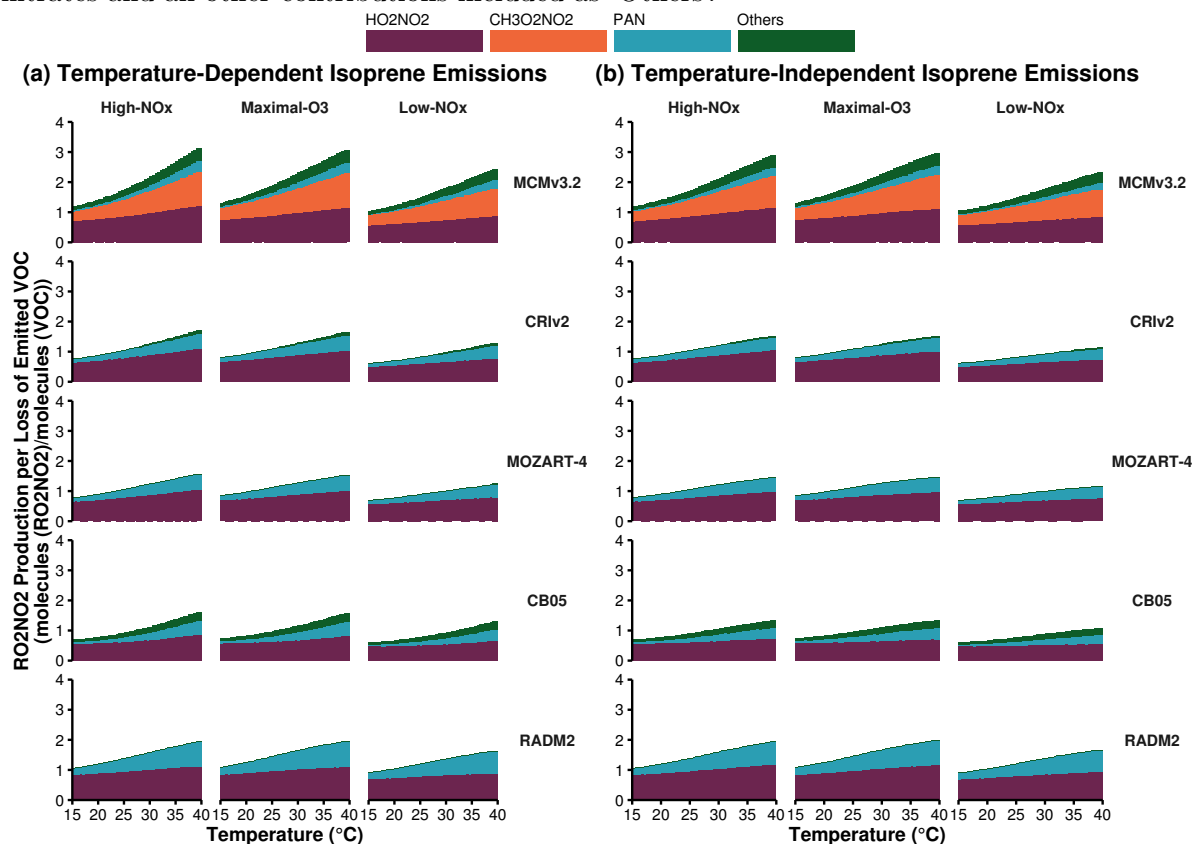
We shall now turn our focus to the peroxy nitrate (RO_2NO_2) contribution as this category has a strongly temperature-dependent contribution to the normalised O_x production. Peroxy nitrates are an important reservoir species for both peroxy radicals and NO_x that are formed from the reactions of alkyl and acyl peroxy nitrates with NO_2 (Reaction R1).



The chemical bond of RO_2NO_2 is quite weak with thermal decomposition being the most important chemical reaction and thermal decomposition depends strongly on temperature. At low temperatures, RO_2NO_2 can accumulate and be transported downwind of emissions of the sources of its precursors (NMVOC and NO_x), after thermal decomposition the release of NO_2 and peroxy radicals can promote production of O_3 downwind (Moxim et al., 1996).

Peroxy nitrates are formed from both alkyl and acyl peroxy radicals, with the acyl peroxy radicals being more thermally stable than the alkyl peroxy nitrates. The most important alkyl peroxy nitrates are pernitric acid (HO_2NO_2) and methylperoxy nitrate ($\text{CH}_3\text{O}_2\text{NO}_2$), while peroxy acetyl nitrate (PAN, $\text{CH}_3\text{C}(\text{O})\text{O}_2\text{NO}_2$) and peroxy propionyl nitrate (PPN, $\text{C}_2\text{H}_5\text{C}(\text{O})\text{O}_2\text{NO}_2$) are important acyl peroxy nitrates.

Figure 5: Day-time RO_2NO_2 production budgets normalised by the total oxidation rate of emitted VOC in the NO_x -regimes of Fig. 2. The total budgets are allocated to the most important peroxy nitrates and all other contributions included as ‘Others’.



The alkyl peroxy nitrates have a weaker $\text{RO}_2\text{—NO}_2$ bond than acyl peroxy nitrates hence alkyl peroxy nitrates have a shorter lifetime than acyl peroxy nitrates. For example, $\text{CH}_3\text{O}_2\text{NO}_2$ has a lifetime of 0.5 seconds at 298 K while PAN has a lifetime of 51 minutes at 298 K (Orlando and Tyndall, 2012).

Each chemical mechanism used in our study represents HO_2NO_2 and PAN, although in many reduced chemical mechanisms PAN represents $\text{CH}_3\text{C}(\text{O})\text{O}_2\text{NO}_2$ and other acyl peroxy nitrates. This representation of PAN in reduced chemical mechanisms can lead to overestimations of PAN levels compared to more detailed chemical mechanisms (Luecken et al., 1999). The near-explicit MCMv3.2 represent a diverse range of peroxy nitrates including $\text{CH}_3\text{O}_2\text{NO}_2$ and about 280 acyl peroxy nitrates.

Figure 5 displays the normalised production budgets of RO_2NO_2 by the total loss rate of the emitted NMVOC, similar to Fig. 4 for each chemical mechanism in each NO_x regime and when using a temperature-independent and temperature-dependent source of isoprene emissions. The large contribution of $\text{CH}_3\text{O}_2\text{NO}_2$ in MCMv3.2 is not mirrored in any reduced chemical mechanism as $\text{CH}_3\text{O}_2\text{NO}_2$ is not represented in any of the reduced chemical mechanisms. In

fact the number of molecules of RO_2NO_2 per molecules of NMVOC oxidised in each reduced chemical mechanism is very similar to that of MCMv3.2 less the contribution of $\text{CH}_3\text{O}_2\text{NO}_2$ for the separate NO_x regimes and regardless of isoprene source.

The contribution of RO_2NO_2 to the normalised O_x production in Fig. 4 is largest in the MCMv3.2 than the reduced chemical mechanisms due to the representation of $\text{CH}_3\text{O}_2\text{NO}_2$ in the MCMv3.2. If reduced chemical mechanisms represent $\text{CH}_3\text{O}_2\text{NO}_2$ chemistry then this would improve the representation of the total RO_2NO_2 production which would have the added effect of improving the representation of O_x production budgets.

4 Discussion

4.1 Ozone Contours

The ozone contours of Fig.2 illustrate the non-linear relationship of ozone mixing ratios to NO_x and temperature which is similar to the contours of ozone production to NO_x mixing ratios and temperature demonstrated in Pusede et al. (2014). The relationship determined in Pusede et al. (2014) is relevant to the San Joaquin Valley, California and was inferred using observational methods.

As highlighted by the review of Pusede et al. (2015) the dependence of ozone to temperature is multi-faceted and is influenced by increased emissions, in particular BVOC such as isoprene emitted from biogenic species, and increased rates of chemical reactions. The increase in isoprene emissions with temperature is shown to be the more important than the increase of ozone production chemistry through increased reaction rates in Fig. 2, as here there is a large increase in ozone at higher temperatures with increased isoprene emissions alone rather than the increased chemistry.

In order to determine how important the effect of increasing isoprene emissions with temperature are in relation to increases in ozone production chemistry, we repeated the sets of model runs at each NO_x condition and temperature using a constant source of isoprene equal to that emitted at the lowest temperature (288 K) and then the highest temperature (313 K). The results of these model runs show that ...

The increase in ozone with temperature tends to follow the same shape as the increase of isoprene emissions with temperature (Fig. 1), showing that the increase of isoprene emissions with temperature may be the dominant factor of increased ozone with temperature.

4.2 Ozone Budgets

The reaction of CH_3CO_3 with NO has the highest contribution to the total O_x budget at higher temperatures in each NO_x condition in Fig. 4. The main source of CH_3CO_3 is its chemical equilibrium with PAN, in the presence of NO_2 , other than this equilibrium it is the degradation of acetaldehyde (CH_3CHO) that leads to a net source of CH_3CO_3 .

The increased contribution of CH_3CO_3 reaction with NO to O_x production budget is more pronounced in the CB05 and RADM2 chemical mechanisms. Acetaldehyde is included in the NMVOC emissions of each chemical mechanism, however it also has a chemical source from the secondary degradation on many other NMVOC. An increased chemical source of CH_3CHO from the representation of tropospheric degradation chemistry in CB05 and RADM2 could be the cause of the higher ozone mixing ratios when using CB05 and RADM2 chemical mechanisms.

Coates and Butler (2015) have shown that the secondary degradation of the RADM2 species HC3 under-estimates the yields of less-reactive ketones at the expense of increased aldehyde yields. Thus the increased aldehyde yields propagate ozone production through the reactions of the degradation products CH_3CO_3 and the methyl peroxy radical (CH_3O_2) with NO. Moreover, in the CB05, there are no ketone species present in this chemical mechanism and the chemical source of carbonyl species is mainly in the form of aldehydes, leading to a similar propagation of ozone production as described for RADM2. Thus the underestimation or missing representation of the yield of ketone species in the RADM2 and CB05 chemical mechanisms leads to higher ozone production and the larger ozone mixing ratios seen in Fig. 2.

The increased amounts of CH_3CO_3 simulated with RADM2 and CB05 also influences another well-known aspect of the relationship of ozone with temperature, namely that at higher temperatures peroxy nitrates (RO_2NO_2), such as PAN, are no longer a suitable reservoir of peroxy radicals and NO_x due to an increase in PAN decomposition rates with temperature, leading to re-release of peroxy radicals and NO_2 which can then go on to further produce ozone. As the chemistry of RADM2 and CB05 produces more CH_3CO_3 this leads to an increase in the mixing ratios of RO_2NO_2 , mainly PAN in RADM2 and CB05, and so the equilibrium state is shifted in these chemical mechanisms compared to the MCM v3.2, CRI v2 and MOZART-4. This shift in equilibrium state is another pathway for increased ozone production with temperature in the CB05 and RADM2.

4.3 Rate of Change of Ozone with Temperature

5 Conclusions

References

William P. L. Carter, Arthur M. Winer, Karen R. Darnall, and James N. Pitts Jr. Smog chamber studies of temperature effects in photochemical smog. *Environmental Science & Technology*, 13(9):1094–1100, 1979.

J. Coates and T. M. Butler. A comparison of chemical mechanisms using tagged ozone production potential (TOPP) analysis. *Atmospheric Chemistry and Physics*, 15(15):8795–8808, 2015.

John P. Dawson, Peter J. Adams, and Spyros N. Pandis. Sensitivity of ozone to summertime climate in the eastern USA: A modeling case study . *Atmospheric Environment*, 41(7):1494 – 1511, 2007.

L. K. Emmons, S. Walters, P. G. Hess, J.-F. Lamarque, G. G. Pfister, D. Fillmore, C. Granier, A. Guenther, D. Kinnison, T. Laepple, J. Orlando, X. Tie, G. Tyndall, C. Wiedinmyer, S. L. Baughcum, and S. Kloster. Description and evaluation of the Model for Ozone and Related chemical Tracers, version 4 (MOZART-4). *Geoscientific Model Development*, 3(1):43–67, 2010.

Wendy S. Goliff, William R. Stockwell, and Charlene V. Lawson. The regional atmospheric chemistry mechanism, version 2. *Atmospheric Environment*, 68:174 – 185, 2013.

A. Guenther, T. Karl, P. Harley, C. Wiedinmyer, P. I. Palmer, and C. Geron. Estimates of global terrestrial isoprene emissions using MEGAN (Model of Emissions of Gases and Aerosols from Nature). *Atmospheric Chemistry and Physics*, 6(11):3181–3210, 2006.

A. B. Guenther, X. Jiang, C. L. Heald, T. Sakulyanontvittaya, T. Duhl, L. K. Emmons, and X. Wang. The Model of Emissions of Gases and Aerosols from Nature version 2.1 (MEGAN2.1): an extended and updated framework for modeling biogenic emissions. *Geoscientific Model Development*, 5(6):1471–1492, 2012.

Shiro Hatakeyama, Hajime Akimoto, and Nobuaki Washida. Effect of temperature on the formation of photochemical ozone in a propene-nitrogen oxide (NO_x)-air-irradiation system. *Environmental Science & Technology*, 25(11):1884–1890, 1991.

369 Daniel J. Jacob and Darrell A. Winner. Effect of climate change on air quality. *Atmospheric*
 370 *Environment*, 43(1):51 – 63, 2009. Atmospheric Environment - Fifty Years of Endeavour.

371 M.E. Jenkin, L.A. Watson, S.R. Utembe, and D.E. Shallcross. A Common Representative
 372 Intermediates (CRI) mechanism for VOC degradation. Part 1: Gas phase mechanism development.
 373 *Atmospheric Environment*, 42(31):7185 – 7195, 2008.

374 J. J. P. Kuenen, A. J. H. Visschedijk, M. Jozwicka, and H. A. C. Denier van der Gon.
 375 TNO-MACC_II emission inventory; a multi-year (2003–2009) consistent high-resolution european
 376 emission inventory for air quality modelling. *Atmospheric Chemistry and Physics*, 14(20):
 377 10963–10976, 2014.

378 AsM Lourens. *Air quality in the Johannesburg-Pretoria megacity: its regional influence and*
 379 *identification of parameters that could mitigate pollution*. PhD thesis, North-West University,
 380 Potchefstroom Campus, 2012.

381 D.J. Luecken, G.S. Tonnesen, J.E. Sickles, and II. Differences in noy speciation predicted by
 382 three photochemical mechanisms. *Atmospheric Environment*, 33(7):1073 – 1084, 1999.

383 W. J. Moxim, H. Levy, and P. S. Kasibhatla. Simulated global tropospheric PAN: Its transport
 384 and impact on NO_x. *Journal of Geophysical Research: Atmospheres*, 101(D7):12621–12638, 1996.

385 John J. Orlando and Geoffrey S. Tyndall. Laboratory studies of organic peroxy radical chemistry:
 386 an overview with emphasis on recent issues of atmospheric significance. *Chem. Soc. Rev.*, 41:
 387 6294–6317, 2012.

388 N. Passant. Speciation of UK emissions of non-methane volatile organic compounds. Technical
 389 report, DEFRA, Oxon, UK., 2002.

390 George Pouliot, Hugo A.C. Denier van der Gon, Jeroen Kuenen, Junhua Zhang, Michael D. Moran,
 391 and Paul A. Makar. Analysis of the emission inventories and model-ready emission datasets of
 392 Europe and North America for phase 2 of the AQMEII project. *Atmospheric Environment*, 115:
 393 345–360, 2015.

394 S. E. Pusede, D. R. Gentner, P. J. Wooldridge, E. C. Browne, A. W. Rollins, K.-E. Min, A. R.
 395 Russell, J. Thomas, L. Zhang, W. H. Brune, S. B. Henry, J. P. DiGangi, F. N. Keutsch, S. A.
 396 Harrold, J. A. Thornton, M. R. Beaver, J. M. St. Clair, P. O. Wennberg, J. Sanders, X. Ren,
 397 T. C. VandenBoer, M. Z. Markovic, A. Guha, R. Weber, A. H. Goldstein, and R. C. Cohen.

398 On the temperature dependence of organic reactivity, nitrogen oxides, ozone production, and
 399 the impact of emission controls in San Joaquin Valley, California. *Atmospheric Chemistry and*
 400 *Physics*, 14(7):3373–3395, 2014.

401 Sally E. Pusede, Allison L. Steiner, and Ronald C. Cohen. Temperature and Recent Trends in
 402 the Chemistry of Continental Surface Ozone. *Chemical Reviews*, 115(10):3898–3918, 2015.

403 D. J. Rasmussen, Jianlin Hu, Abdullah Mahmud, and Michael J. Kleeman. The ozone–climate
 404 penalty: Past, present, and future. *Environmental Science & Technology*, 47(24):14258–14266,
 405 2013. PMID: 24187951.

406 Andrew Rickard, Jenny Young, M. J. Pilling, M. E. Jenkin, Stephen Pascoe, and S. M. Saunders.
 407 The Master Chemical Mechanism Version MCM v3.2. <http://mcm.leeds.ac.uk/MCMv3.2/>,
 408 2015. [Online; accessed 25-March-2015].

409 Sanford Sillman. The use of NO_y, H₂O₂, and HNO₃ as indicators for ozone-NO_x-hydrocarbon
 410 sensitivity in urban locations. *Journal of Geophysical Research: Atmospheres*, 100(D7):
 411 14175–14188, 1995.

412 Sanford Sillman. The relation between ozone, NO_x and hydrocarbons in urban and polluted
 413 rural environments. *Atmospheric Environment*, 33(12):1821 – 1845, 1999.

414 Sanford Sillman and Perry J. Samson. Impact of temperature on oxidant photochemistry in
 415 urban, polluted rural and remote environments. *Journal of Geophysical Research: Atmospheres*,
 416 100(D6):11497–11508, 1995.

417 D. Simpson, A. Benedictow, H. Berge, R. Bergström, L. D. Emberson, H. Fagerli, C. R. Flechard,
 418 G. D. Hayman, M. Gauss, J. E. Jonson, M. E. Jenkin, A. Nyíri, C. Richter, V. S. Semeena,
 419 S. Tsyro, J.-P. Tuovinen, Á. Valdebenito, and P. Wind. The EMEP MSC-W chemical transport
 420 model – technical description. *Atmospheric Chemistry and Physics*, 12(16):7825–7865, 2012.

421 William R. Stockwell, Paulette Middleton, Julius S. Chang, and Xiaoyan Tang. The second
 422 generation regional acid deposition model chemical mechanism for regional air quality modeling.
 423 *Journal of Geophysical Research: Atmospheres*, 95(D10):16343–16367, 1990.

424 William R. Stockwell, Frank Kirchner, Michael Kuhn, and Stephan Seefeld. A new mechanism
 425 for regional atmospheric chemistry modeling. *Journal of Geophysical Research: Atmospheres*,
 426 102(D22):25847–25879, 1997.

427 E. von Schneidemesser, J. Coates, A. J. H. Visschedijk, H. A. C. Denier van der Gon, and T. M.
428 Butler. Variation of the NMVOC speciation in the solvent sector and the sensitivity of modelled
429 tropospheric ozone. *Atmospheric Environment*, page In preparation, 2015.

430 Greg Yarwood, Sunja Rao, Mark Yocke, and Gary Z. Whitten. Updates to the Carbon Bond
431 Chemical Mechanism: CB05. Technical report, U. S Environmental Protection Agency, 2005.